agronomy

MDPI

Article

Detecting Irrigation Events over Semi-Arid and Temperate Climatic Areas Using Sentinel-1 Data: Case of Several Summer Crops

Hassan Bazzi [1,2,*], Nicolas Baghdadi [1,*], Sami Najem [1], Hadi Jaafar [3], Michel Le Page [4], Mehrez Zribi [4], Ioannis Faraslis [5] and Marios Spiliotopoulos [6]

[1] INRAE, UMR TETIS, University of Montpellier, AgroParisTech, 500 Rue François Breton, CEDEX 5, 34093 Montpellier, France
[2] Atos France, Technical Services, 80 Quai Voltaire, 95870 Bezons, France
[3] Department of Agriculture, American University of Beirut, Beirut 2020-1100, Lebanon
[4] CESBIO (CNES/CNRS/INRAE/IRD/UPS), 18 av. Edouard Belin, bpi 2801, CEDEX 09, 31401 Toulouse, France
[5] Department of Environmental Sciences, School of Technology, University of Thessaly, 41500 Larissa, Greece
[6] Department of Civil Engineering, School of Engineering, University of Thessaly, 38334 Volos, Greece
* Correspondence: hassan.bazzi@atos.net (H.B.); nicolas.baghdadi@teledetection.fr (N.B.)

Abstract: Irrigation monitoring is of great importance in agricultural water management to guarantee better water use efficiency, especially under changing climatic conditions and water scarcity. This study presents a detailed assessment of the potential of the Sentinel-1 (S1) Synthetic Aperture Radar (SAR) data to detect irrigation events at the plot scale. The potential of the S1 data to detect the irrigation events was carried out using the Irrigation Event Detection Model (IEDM) over semi-arid and temperate oceanic climates in five study sites in south Europe and the Middle East. The IEDM is a decision tree model initially developed to detect irrigation events using the change detection algorithm applied to the S1 time series data. For each study site and at each agricultural plot, all available S1 images during the period of irrigation were used to construct an S1 time series and apply the IEDM. Different types of major summer irrigated crops were analyzed in this study, including Maize, Soybean, Sorghum and Potato, mainly with the sprinkler irrigation technique. The irrigation detection accuracy was evaluated using S1 images and the IEDM against the climatic condition of the studied area, the vegetation development (by means of the normalized difference vegetation index, NDVI) and the revisit time of the S1 sensor. The main results showed generally good overall accuracy for irrigation detection using the S1 data, reaching 67% for all studied sites together. This accuracy varied according to the climatic conditions of the studied area, with the highest accuracy for semi-arid areas and lowest for temperate areas. The analysis of the irrigation detection as a function of the crop type showed that the accuracy of irrigation detection decreases as the vegetation becomes well developed. The main findings demonstrated that the density of the available S1 images in the S1 time series over a given area affects the irrigation detection accuracy, especially for temperate areas. In temperate areas the irrigation detection accuracy decreased from 70% when 15 to 20 S1 images were available per month to reach less than 56% when less than 10 S1 images per month were available over the study sites.

Keywords: remote sensing; precision agriculture; sustainability; climate change

Citation: Bazzi, H.; Baghdadi, N.; Najem, S.; Jaafar, H.; Le Page, M.; Zribi, M.; Faraslis, I.; Spiliotopoulos, M. Detecting Irrigation Events over Semi-Arid and Temperate Climatic Areas Using Sentinel-1 Data: Case of Several Summer Crops. *Agronomy* **2022**, *12*, 2725. https://doi.org/10.3390/agronomy12112725

Received: 9 October 2022
Accepted: 31 October 2022
Published: 3 November 2022

1. Introduction

One of the most important threats of climate change is its impact on the availability of freshwater resources. Globally, the biggest draw of water resources is the agriculture sector, expending around 70% of the total freshwater resources [1–3]. The world's increasing population is adding strain on agricultural production to satisfy the demand for food and

for animal feed. Meeting these growing food needs is pushing decision makers toward intensifying agricultural activity, therefore raising the agriculture water demand for the purpose of irrigation. Irrigation monitoring is essential to support the implementation of water management policies and increase water use efficiency [4–6]. Monitoring irrigation activities does not only include spatial quantification of the irrigated areas, but also gathering knowledge about the frequency of irrigation and the corresponding water consumption [6–10].

At larger scales, remote sensing is a powerful tool for land surface monitoring. The Earth Observation (EO) data available now at enormous spatial scales makes it possible to achieve land surface monitoring, including and not limited to several agricultural and hydrological applications [11–15]. Remote sensing has proven its great potential and efficiency in irrigation applications where several techniques and models were developed to produce irrigation maps and the detection of the frequency of irrigation, as well as for the estimation of the irrigation water consumption at the local, regional and national scales. The large-scale monitoring of irrigation, at national and regional scales, is beneficial to estimate accurate irrigation water consumption, which in return could be useful for authorities to detect, follow and reduce the illegal water abstractions from rivers and groundwater aquifers especially in countries that lack precise water consumption declarations by farmers and suffer from water scarcity.

Recently, several studies have exploited Synthetic Aperture Radar (SAR) data and optical data for the monitoring of irrigated areas [7–9,16–23]. The proxy-measure of irrigation (mapping and irrigation frequency) using SAR data relies on the variation in the surface soil moisture (SSM), which has been demonstrated to correlate well with radar backscattering coefficients [24–29]. On the other hand, optical data were commonly used to map the irrigated surface using the difference in the spectral signature between irrigated and rain-fed areas. Due to the abundance of water in irrigated plots, they usually harbor more intense photosynthesis and denser biomass, thus leading to differences in the spectral signature between irrigated plots and comparable rain-fed plots. These differences are likely visible using vegetation indices derived from multispectral optical satellites such as the normalized difference vegetation index (NDVI), the normalized difference water index (NDWI) and the normalized difference red-edge index (NDRE) [30,31]. The combined use of optical and SAR data proved the capability of obtaining, on one hand, accurate irrigated area maps, as well as precise monitoring of the frequency of irrigation [19,31,32].

Currently, the only SAR and optical EO data that offer continuous monitoring of the land surface at the combined high temporal (five to six days revisit time before the loss of S1B sensor on 3 August 2022) and spatial resolutions (up to 10 m) are the Sentinel-1 and Sentinel-2 satellite data. Where Sentinel-1 ensures continuous SAR imaging for six days of temporal resolution, the Sentinel-2 offers four days of revisit time for optical images. Several studies showed that the C-band (5.405 GHz) SAR time series from the Sentinel-1 (S1) satellite is efficient for mapping irrigated areas and for detecting irrigation frequency (irrigation episodes) [7,16,33]. Models built using the S1 C-band data rely on detecting the changes in the backscattering of the SAR coefficient between consecutive images (at a time difference of six days), such as the one developed by Bazzi et al. [32,33], Le Page et al. [34] and Ouaadi et al. [35], that is basically related to changes in the surface soil moisture (about 3 to 5 cm depth in the C-band). A sharp increase in the backscattering coefficients between two S1 images can be attributed to a sharp increase in surface soil moisture, caused either by an irrigation episode or by a rainfall event. On the other hand, a decrease in the SAR backscattering coefficients between consecutive S1 images is evidence of a decrease in soil moisture values and thus the absence of any water input caused by either rainfall or irrigation. Since models built using S1 data for irrigation detection rely on change detection between the consecutive S1 images, the revisit time of the satellite is the most important factor that limits the irrigation detection capability. In fact, after a wetting event (irrigation, rainfall), the surface soil moisture evaporates in a few days. If SSM increased from 15–20 vol.% to 30–40 vol.% with the wetting event, it returns to 15–20 vol.% after about

three days (in the case of loam soil texture [28,36]). However, the rate of drying out of the soil following a wetting event (days needed to dry out completely) may vary according to on the soil texture.

In the context of agricultural areas, the effect of vegetation cover on the SAR backscattering signal cannot be disregarded. In fact, the penetration of the SAR signal through the canopy cover to reach the soil layer and detect soil moisture information is highly dependent on the characteristics of the vegetation canopy: characteristics such as structure, biomass, vegetation water content and vegetation density. There are other factors affecting SAR penetration through vegetation, specifically, the SAR wavelength used. Bazzi et al. [37] analyzed the sensitivity of the SAR signal in C- (wavelength ~6 cm) and L-bands (wavelength ~24 cm) for the detection of the irrigation events. They concluded that when the vegetation is moderately developed (NDVI $\leq$ 0.7), the C-band temporal variation remains sensitive to the soil moisture dynamics and the irrigation events can be detected. However, a well-developed vegetation cover constrains the detection of irrigation when using the C-band wavelength for a few crop types. They showed that over Gramineae (cereal) crops (such as Wheat and Barley) the SAR backscattering response to the irrigation event was negligible when the vegetation was highly developed. However, legume crop types did not show any constraint for irrigation detection using the C-band SAR signal even in the presence of well-developed vegetation cover. On the other hand, the L-band with a higher wavelength did not show any limitation in the irrigation detection in the presence of well-developed vegetation cover. In the same context, El Hajj et al. [36] showed for LAI (leaf area index) values beyond 1.5 m^2/m^2 with a vegetation height of approximately 70 cm in Wheat crops, the C-band S1-SAR signal in VV and VH polarizations becomes insensitive to surface soil moisture. Similarly, Baghdadi et al. [38] also showed that the sensitivity of the SAR signal in the C-band (VV polarization) decreases from 0.11 dB/vol.% for low biomass values to 0.05 dB/vol.% for biomass values greater than 1 kg/m^2 (NDVI ~0.7).

In a recent study, Bazzi et al. [33] proposed an algorithm called the IEDM (Irrigation Event Detection Model) to detect irrigation events at the plot scale. This algorithm mainly relies on the change detection in the S1 C-band backscattering coefficients where the increase in the SAR backscattering coefficient is mainly due to the increase in the soil moisture values caused either by a rainfall event or by an irrigation episode. To separate irrigation from rainfall, they compared the S1 backscattering signal at the plot scale to that at the basin scale (grid scale of 10 km $\times$ 10 km). The assumption says that if the increase in the plot scale backscattering coefficient is due to rainfall, all the surrounding plots must encounter the same variation and therefore the SAR backscattering at grid scale would also increase. On the other hand, the occurrence of an irrigation episode would affect only the targeted plot, thus the increase in the SAR signal at the plot scale accompanied with a stability or decrease at grid scale is evidence of a local change in soil moisture at the plot level, and thus it is the effect of irrigation and not rainfall [7,14]. In Bazzi et al. [33], they proposed that the IEDM could be suitable for operational near-real-time application for irrigation detection at the plot scale.

The integration of the IEDM as an operational tool to detect irrigation events in a near-real-time scenario requires first a deep assessment of the strength and limitations of the IEDM. Our objective in this study is to assess the feasibility of using the IEDM and S1 time series for irrigation detection by considering the maximum likelihoods that may be encountered in an operational application of the IEDM mainly regarding the climatic conditions and the crop type. To do so, we collected a wide database of irrigation that contains irrigation data from different climatic regions and over several summer crops. This kind of assessment may help understand the applicability of the IEDM at large scales. The study was carried out over five study sites in Tarn, France; West Occitanie, France; East Occitanie, France; Bekaa Valley, Lebanon; and the Thessaly region, Greece. Crop types included common summer irrigated crops such as Maize, Soybean, Sorghum and Potato. The climate among sites varies from semi-arid to temperate. The IEDM was applied at the agricultural plot scale and the accuracy of irrigation detection was analyzed according

to the climatic conditions, vegetation development and the frequency of the available S1 images (S1 orbits and S1 revisit time).

2. Materials and Methods

2.1. Study Sites and In Situ Datasets

The assessment of the Irrigation Event Detection Model (IEDM) developed by Bazzi et al. [33] was carried out over five study sites located in Tarn, France (TR), West Occitanie, France (OW), East Occitanie, France (OE), Bekaa Valley, Lebanon (LB), and the Thessaly region, Greece (GR), across several years depending on the data availability in each site (Figure 1 and Table 1). The studied sites belong to two different climatic zones. According to the Koppen Geiger climate classes, the GR, LB and OE sites correspond to the hot summer Mediterranean climate (Csa) also known as the typical Mediterranean climate, with an annual precipitation below 600 mm. The OW and TR sites correspond to the temperate oceanic climate (Cbf according to Koppen Geiger climate classification), with an annual precipitation over 800 mm. Crop types in this study across the studied sites are Maize, Soybean, Sorghum and Potato. As shown in Table 1, the irrigation period is usually between May and October, corresponding to the summer crop irrigation. The common irrigation method between all sites is the sprinkler irrigation method, except for the GR site where both sprinkler and drip irrigations are used during the irrigation season.

Figure 1. Location of study sites. Same-colored boxes and dots correspond to the same location. In green (LB), in red (GR), in blue (OE), in yellow (TR) and in magenta (OW).

2.2. Sentinel-1 (S1) Synthetic Aperture Radar (SAR) Time Series

In this study, the time series of C-band (5.405 GHz) S1 SAR images acquired by S1A and S1B satellites was used in both "ascending" (afternoon at 18:00 UT) and "descending" (morning at 06:00 UT) acquisitions in the Vertical–Vertical (VV) and the Vertical–Horizontal (VH) polarizations. The pixel spacing of the S1 images was 10 m × 10 m. The images were downloaded from the European Space Agency's (ESA) website (https://scihub.copernicus.eu/dhus/#/home (accessed on 1 November 2022)) and calibrated using the S1

toolbox developed by ESA. The calibration process (radiometric and geometric calibrations) converts the data from a digital number into a backscattering coefficient in linear units (radiometric calibration). It also ortho-rectifies the images (geometric calibration) using a digital elevation model at 30 m from the Shuttle Radar Topography Mission (SRTM).

Table 1. Plots' characteristics, crop types and irrigation information over the study sites.

Site	Crop Type	Year	Number of Plots	Total Number of Irrigations	Irrigation Period	Average Plot Size (Ha)
TR	Maize	2017	7	51	09/06–29/08	11.2
TR	Maize	2018	7	34	22/06–29/08	8.41
TR	Maize	2019	7	42	16/06–06/08	6.5
TR	Soybean	2017	2	8	22/06–28/08	6.3
TR	Soybean	2018	2	15	30/06–08/09	10.4
TR	Soybean	2019	3	20	30/06–18/09	11.04
OW	Soybean	2020	4	21	09/06–05/09	0.96
OE	Maize	2017	1	30	09/05–13/10	1.2
OE	Soybean	2017	1	13	09/05–13/10	0.8
OE	Sorghum	2017	1	5	09/05–13/10	0.44
LB	Potato	2020	1	12	06/08–10/11	1.70
GR	Maize	2021	2	22	24/05–10/08	2.03

Across our study sites, different numbers of S1 images could be obtained depending on the path of the S1 orbit and on the overlapping area between the S1 orbits. In ideal cases, a total of 20 S1 images per month could be obtained for a study site with 4 S1 images from 4 S1 orbits in a period of 6 days. However, some studied sites had less images per month due to two main reasons. Firstly, sometimes the four orbits do not overlap over the study site and thus less orbits could be used. Second, some S1 images from either S1A or S1B satellites were not available, probably due to technical acquisition problems. Table 2 summarizes the maximum number of the S1 images obtained at each site/year.

Table 2. The number of available S1 images per site and year.

Site	Year	Total Number of Images	Total Number of Orbits	Number of Images per Month
TR	2017	121	2	10
TR	2018	98	2	8
TR	2019	84	2	7
OW	2020	239	4	20
OE	2017	121	2	10
LB	2020	179	3	15
GR	2021	238	4	20

2.3. Sentinel-2 (S2) Optical Time Series

All available Sentinel-2 (S2) optical images over each study site/year were downloaded from the Theia website (https://www.theia-land.fr/ (accessed on 1 November 2022)). S2 images cover the same time span of the S1 acquisitions for each site/year. Cloud-free optical images are available at a frequency of approximately two images per month. The S2 images provided by Theia are corrected for atmospheric interference and so are called Level-2A products. S2 images were mainly used to calculate the NDVI time series needed for the IEDM application and the analysis of the IEDM.

2.4. Irrigation Event Detection Model (IEDM)

2.4.1. Description of the IEDM

In a recent study, Bazzi et al. [33] proposed a decision tree algorithm called the IEDM (Irrigation Event Detection Model) for detecting irrigation events at plot scale using mainly the S1 time series data. The IEDM detects the change in the SAR backscattering coefficients at plot scale (σ^0_{plot}) and compares it to the σ^0 values derived at basin or grid scales σ^0_{Grid}. It assumes first that when the surface soil moisture at the plot increases between two consecutive S1 acquisitions, the σ^0_{plot} value between these two dates increases. However, the increase in the σ^0_{plot} value could be due to either rainfall or irrigation. Thus, the challenge was to discriminate the increase in the σ^0_{plot} due to irrigation from that due to rainfall events. To overcome this limitation, Bazzi et al. [33] proposed to conjointly use the σ^0_{Grid} at 10 km scale with the σ^0_{plot}. The σ^0_{Grid} values are calculated as an average of the S1 backscattering at 10 km grid scale only for bare soil agricultural plots with low vegetation cover. Bare soil agricultural plots are usually extracted using the winter and summer crop classes of a land cover map [39] (excluding orchards) and a simple NDVI thresholding (NDVI < 0.4). They suppose that when a rainfall event occurs between two S1 images, all the bare soil agricultural plots within a given radius (e.g., 10 km × 10 km) must show an increase in their soil moisture values and consequently in their σ^0_{plot} value. Thus, due to a rainfall event between two S1 images, the average σ^0 calculated for all the bare soil plots within a 10 km grid cell (σ^0_{Grid}) would increase. This correlation between soil moisture at grid scale and rainfall was also demonstrated by Bazzi et al. [14]. In the IEDM, the increase in the soil moisture values at an agricultural plot due to irrigation was detected by comparing the increase in the σ^0_{plot} to that in the σ^0_{Grid}. When both σ^0_{plot} and σ^0_{Grid} increase simultaneously between the two S1 images then a rainfall event occurred, and if an irrigation event had also occurred it could not be detected. When the σ^0_{plot} increases between two S1 images and the σ^0_{Grid} value decreases or remains stable at low levels (stable and low σ^0_{Grid} values mean persistence of dry conditions), then an irrigation event most likely occurred at the plot.

For each agricultural plot and at each S1 image, the IEDM gives an irrigation likelihood score of 0, 25, 50 or 100. The four irrigation possibility values are directly related to the change in the σ^0_{plot} (plot scale) and σ^0_{Grid} (grid scale) values between two dates t_i and t_{i-1}: $\Delta\sigma^0_{plot} = \sigma^0_{plot}(t_i) - \sigma^0_{plot}(t_{i-1})$ and $\Delta\sigma^0_{Grid} = \sigma^0_{Grid}(t_i) - \sigma^0_{Grid}(t_{i-1})$.

- The value 0 corresponds to the absence of any irrigation chance between t_i and t_{i-1} due to either decrease in the σ^0_{plot} ($\Delta\sigma^0_{plot} \leq -0.5$ dB) or increase in the $\Delta\sigma^0_{Grid}$ ($\Delta\sigma^0_{Grid} \geq 1$ dB rainfall event occurred).
- The low irrigation possibility weight (value = 25) corresponds to the absence of rainfall events between t_i and t_{i-1} ensured by the stability or the decrease in σ^0_{Grid} ($\Delta\sigma^0_{Grid} \leq 0.5$ dB) and a slight modification in the σ^0_{plot} between t_i and t_{i-1} ($-0.5 \leq \Delta\sigma^0_{plot} < 0.5$ dB), meaning that an irrigation event might have occurred at the beginning of the period.
- The medium irrigation possibility weight (value = 50) is associated with a moderate increase in the σ^0_{plot} ($0.5 \leq \Delta\sigma^0_{plot} < 1$ dB).
- The high possibility of irrigation (value = 100) is ensured when the σ^0_{plot} strongly increases ($\Delta\sigma^0_{plot} \geq 1$ dB) with the absence of rainfall events between t_i and t_{i-1} ensured by the stability or the decrease in σ^0_{Grid} ($\Delta\sigma^0_{Grid} \leq 0.5$ dB)

In addition to the major filters discussed above, the IEDM uses some auxiliary filters to confirm the existence of an irrigation event or to remove falsely detected irrigation events. One of the additional filters considers the surface soil moisture estimations at plot scale estimated using the neural network proposed by [26]. For example, when the σ^0_{plot} slightly increases between t_i and t_{i-1}, the IEDM uses the soil moisture estimation at plot scale to confirm the existence of low irrigation possibility weight (value = 25). If the plot's soil

moisture estimation at time t_{i-1} is high ($\geq$20 vol.%) due to either rainfall or irrigation and remains with high value to time t_i without rainfall event detected by σ^0_{Grid} (temperate soil conditions persisted from time t_{i-1} to t_i), then the irrigation at low possibility is confirmed. Moreover, a filter using the NDVI time series is applied to reduce some falsely detected irrigation events. These false detections could be due to the increase in the σ^0_{plot} values related to the change in surface roughness or vegetation cover. The NDVI filter proposes that if an event is detected with low NDVI value at date t_i (NDVI < 0.4) and the NDVI value one month later at t_{i+30} decreases or remains stable (NDVI (t_{i+30}) − NDVI $(t_i) \leq 0.1$), then the event is discarded (crop cycle in decreasing stage or persistent bare soil conditions). For a detailed description of the IEDM including all the criteria of the decision tree, the reader is referred to the study of Bazzi et al. [33] that deeply describes the IEDM algorithm.

2.4.2. Application of the IEDM at Plot Scale

IEDM was applied independently for each plot, orbit and polarization (VV and VH). Two reasons are behind applying the IEDM on each orbit separately (image every six days) instead of mixing all the images from all orbits in one time series (two to four images every six days). As stated in Bazzi et al. [33], the first reason is that the incidence angle varies between different orbits (incidence angle varies between 30° and 45°) and the normalization of the incidence angle can add another source of undesirable error on the time series. Second, the diurnal variation, which is the result of the difference in the vegetation water content (VWC) between the morning and the evening, causes high difference in the radar backscattering signal over vegetated plots between the morning and the evening acquisitions. Exact quantification of the diurnal effect is not yet assessed, and therefore joining the evening and the morning acquisition may lead to several fluctuations in the SAR time series related to the diurnal effect and not to the soil moisture variation.

Considering that a plot is covered by (m) orbits (m between two and four orbits) with (pol) polarizations (pol = 2, VV and VH), a result of (m × pol) labeled irrigation possibility time series could be obtained at each plot. For example, a plot covered by four orbits in VV and VH polarization would have a total of eight time series data of labeled likelihood irrigation possibilities. The irrigation possibilities at each orbit are at six days revisit (same revisit of the S1 images).

Combining the (m × pol) time series data in only one time series of irrigation possibilities was performed as suggested by Bazzi et al. [8,32] (Figure 2). For each group of S1 images originating from different orbits in a six-day interval (two to four images in six days depending on the number of orbits), the irrigation possibilities are summed for these images in VV and VH separately (P_{VV} and P_{VH}). Then, P_{VV} and P_{VH} are summed for the same time window to obtain one p value, if and only if both P_{VV} and P_{VH} are greater than 0. Otherwise, the p value of this time window is set to 0. As proposed by Bazzi et al. [32], a threshold value of 100 was fixed to compare the resultant p value and judge whether an irrigation event is detected or not in this time interval. The time interval is considered to have a detected irrigation event if it attains a $P \geq 100$. In this case, we say that an irrigation event exists within this six-day interval. The six-day intervals registering detected irrigation possibilities ($P \geq 100$) are then compared to the in situ irrigation events. First, the irrigation dataset is harmonized with the 6-day revisit time of the S1 satellite to consider that if several irrigation events on the same plot occur between the same 6-day interval, these irrigation events are considered as only one irrigation event. True detected irrigation events are thus the irrigation events that lie in time within their corresponding intervals having a $P \geq 100$. A false detection irrigation event is thus the six-day time intervals that have $P \geq 100$ but no in situ irrigation is recorded. Finally, missed irrigation (undetected irrigation event) is an irrigation event that lies within a time interval that registered no value for irrigation possibility (Figure 2).

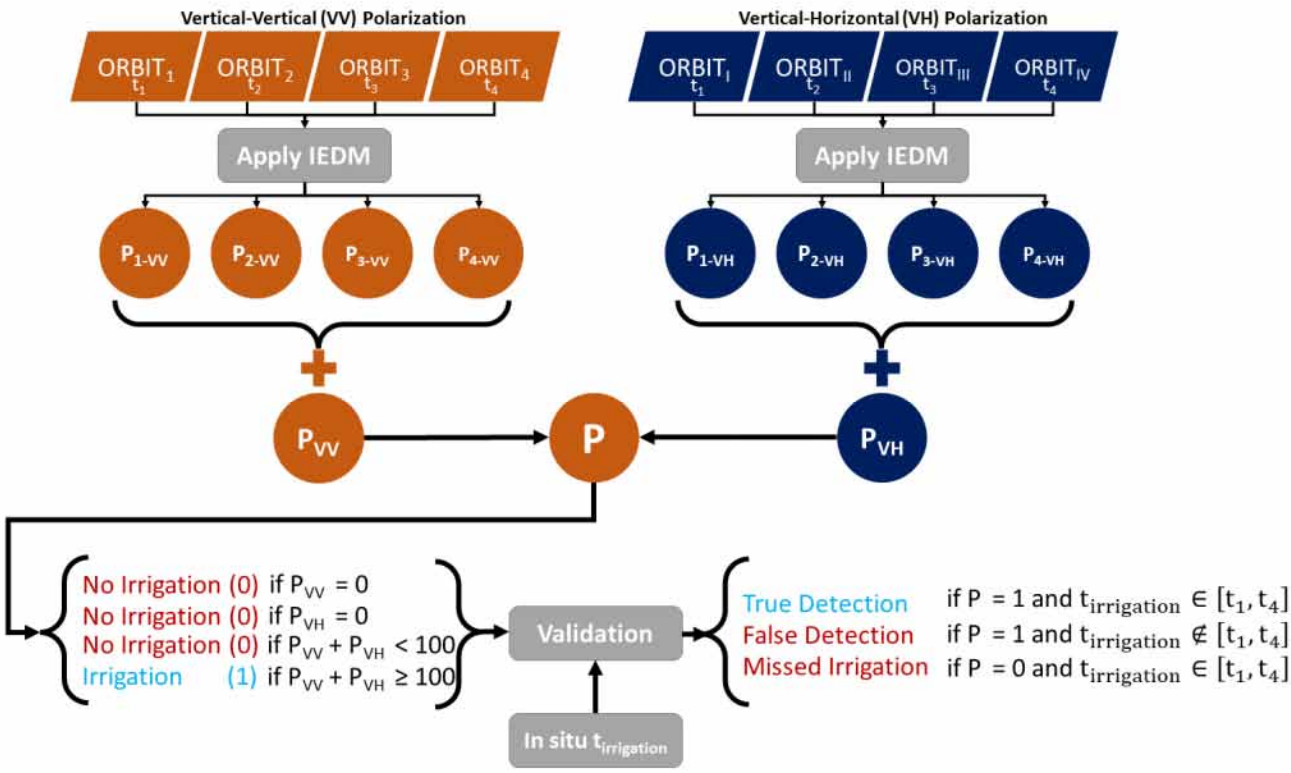

Figure 2. Flowchart of the application of IEDM and the combination of the irrigation likelihood for each group of S1 images originating from different orbits in a six-day interval; t_1, t_2, t_3 and t_4 correspond to the maximum dates of the 4 S1 images in a 6-day time interval and $t_{irrigation}$ corresponds to the in situ registered irrigation date.

The recall, precision and F-score were calculated to evaluate the accuracy of the IEDM for irrigation detection. The three metrics were calculated at the level of crop type for each site/year. Thus, all the detected, undetected and falsely detected events were summed up for all plots of the same crop type in each site/year and the three metrics were calculated.

The recall values reflect the ratio of true positive detections by IEDM over the total number of real irrigations over the plot. High recall value means a large part of the irrigations was successfully detected:

$$\text{Recall} = \frac{\text{Number of True Positive detections}}{\text{Total number of real irrigations}} \times 100\%$$

The precision value is the number of true-positive detections over the total number of detected events (true and false detection). A high precision means there is less possibility of having a false detection (detecting an irrigation that did not occur):

$$\text{Precision} = \frac{\text{Number of True Positive detections}}{\text{Total number of detection}} \times 100\%$$

The F-score combines both the recall and the precision values, allowing for a more global understanding of the accuracy. The higher the F-score, the better the performance is:

$$\text{F} - \text{score} = \frac{2 \times \text{Recall} \times \text{Precision}}{\text{Recall} + \text{Precision}} \times 100\%$$

3. Results

3.1. IEDM Accuracy for Irrigation Detection

Table 3 summarizes the recall, precision and F-score values of each study site at each year and for each specific crop type. In the Tarn study (temperate climate), the recall values

of the Maize crop ranged between 43% and 57% between 2017 and 2019 with an F-score value reaching 64% in 2019 and its lowest value in 2018 (51%). The Soybean crops showed generally lower recall and F-score values in Tarn compared to Maize across the three years, with recall values ranging between 31% and 63% and an F-score between 42% and 59%. This indicates that generally, over Tarn the model performed better on Maize than on Soybean for three years with one out of two irrigations not detected. The four Soybean plots in the OW site (temperate climate) in 2020 with a total of 20 irrigation events showed a recall value of 66%, indicating the proper detection of 14 out of the 21 irrigation events. An additional four false-detected events on the four plots (average of one false detection per plot) were detected with a precision value reaching 76%, leading to an F-score of 70%. In the OE site with semi-arid climatic conditions, the results showed better accuracy for the detection of the irrigation events. For the three plots Maize, Soybean and Sorghum, the F-score value reached 89%, 86% and 83%, respectively. High recall and precision values for OE also ensures the good detection of almost all the irrigation events with very few false irrigation detections. The Potato plot in Lebanon's semi-arid region also showed similar results to that of the OE. Out of 12 irrigations, 10 irrigations were correctly detected and only 1 false detection was observed, leading to a recall, precision and F-score of 83%, 91% and 87%, respectively. Similarly, the two Maize plots in Greece with a total of 22 irrigation events had a recall value of 72%, with 16 out of 22 irrigation events detected. Only two false detections were detected on the two plots (average of one false detection per plot), with a precision reaching 84% and an F-score reaching 75%.

Table 3. Recall, precision and F-score per site, year and crop type.

Site	Crop Type	Year	Number of Plots	Total Number of Irrigations	Recall (%)	Precision (%)	F-Score (%)
TR	Maize	2017	7	51	47%	73%	57%
TR	Maize	2018	7	34	43%	63%	51%
TR	Maize	2019	7	42	57%	73%	64%
TR	Soybean	2017	2	8	63%	56%	59%
TR	Soybean	2018	2	15	31%	63%	42%
TR	Soybean	2019	3	20	38%	80%	52%
OW	Soybean	2020	4	21	66%	76%	70%
OE	Maize	2017	1	30	92%	86%	89%
OE	Soybean	2017	1	13	92%	81%	86%
OE	Sorghum	2017	1	5	100%	71%	83%
LB	Potato	2020	1	12	83%	91%	87%
GR	Maize	2021	2	22	72%	84%	75%
	Overall		38	273	60%	76%	67%

Generally, across all sites, years and crop types, 60% of the irrigation events were detected (recall) with a precision of 76% and an F-score of 67%. The overall false detections for all the 38 plots with a total number of irrigations of 273 reached 53 false detections, with an average of 1 to 2 false detections per plot per season (the number of irrigations per plot is between 5 and 30 irrigations depending on crop type and the climatic zone).

3.2. Effect of the Climatic Conditions

The irrigation detection could be limited depending on the studied climatic region. To better understand the effect of the climatic conditions on the detection of the irrigation events, we calculated the accuracy metrics per climatic conditions considering OE, LB and GR as belonging to the arid to semi-arid region and TR and OW as belonging to the temperate region. Data from the two climatic conditions were considered regardless of

the crop type and the studied year, even though both factors play an important role in the irrigation detection. Table 4 shows the recall, precision and F-score calculated per climatic region by considering the sum of all detected, undetected and falsely detected irrigation events in each climatic region. The results clearly show that over the semi-arid climatic conditions better detection of irrigation events is achieved with a recall value reaching 86% (86% of the total irrigation events summed for all semi-arid sites are detected) with an F-score of 85%. Less accuracy is obtained for temperate regions (TR and OW together) where the recall reaches only 49% (approximately half of the irrigation events are detected) and an F-score of 53% (Table 4). These results ensure that in drier conditions, with rare rainfall events in the summer season and generally drier soil, clearer separation between the dry and the wet states could be obtained, and therefore, clearer capture of the increases in soil moisture that are linked to irrigation events could be detected.

Table 4. Recall, precision and F-score per climatic region.

Climate	Recall	Precision	F-Score	% Undetected Irrigations Due to Rainfall
Arid to Semi-Arid	86%	83%	85%	15.3%
Temperate	49%	70%	53%	30.1%

Table 4 also presents the percentage of the irrigation events not detected due to the presence of rainfall events. Among all the undetected irrigation events, the events that were not detected specifically due to the presence of rainfall are counted. Then, the percentage is calculated as the number of irrigation events not detected only due to rainfall divided by the total number of the undetected irrigation events. An irrigation event is considered as undetected due to rainfall if a rainfall event occurs within the same time interval (between consecutive S1 images) as the irrigation event. Rainfall events can be easily determined based on the increase in the grid scale backscattering coefficients ($\Delta\sigma^0_{Grid} \geq 1$ dB) between two S1 images. In the temperate areas, 30.1% of the undetected irrigation events were found to be undetected due to the presence of the rainfall events. Indeed, when both the irrigation event and the rainfall event occur simultaneously between the same S1 acquisition images (at six days revisit), it would be very difficult to distinguish the effect of irrigation from that of the rainfall, since both events cause the increase in the soil moisture values and their effect on the S1 image is the same. Thus, the rainfall justifies approximately 30.1% of the failure to detect the irrigation events in a temperate area. Therefore, in temperate areas encountering frequent rainfall events, the detection of the irrigation event could be highly constrained by rainfall and is not only related to the efficiency of the IEDM in irrigation detection. In contrast, in the arid to semi-arid study zones, 15% of irrigations were missed because of rainfall events, meaning that there were less rainfall events that could negatively affect the accuracy of irrigation detection.

3.3. Effect of the Vegetation Cover

The effect of the vegetation cover in detecting irrigation events could not be discarded, because the C-band SAR signal is sometimes attenuated by the vegetation cover. As such, we analyzed the effect of crop growth on the accuracy of irrigation detection to understand the constraints of vegetation development on the irrigation detection and analyze this constraint as a function of crop type. Since the two dominant crop types are Maize and Soybean, with robust and rich datasets to draw out conclusions, this analysis concentrates on these two crop types. For this reason, plots with these two crop types were grouped together to obtain two groups: Maize and Soybean. Plots are grouped regardless of the climatic region and the studied year, since the importance here is to discuss only the vegetation development, which is expected to be similar for the same crop across regions.

Table 5 summarizes the accuracy metrics (recall, precision, F-score) obtained for these two crop types. The Maize crops show slightly better detection of irrigation events than the Soybean with a precision of 59.7% for Maize and 54.5% for Soybean. Both crop types have nearly similar precision values (around 74–75%). Similar precisions indicate that the crop

type does not induce differences in false detections, which could be more likely attributed to the threshold values of the IEDM and the radiometric accuracy of the S1 data (fluctuation in the S1 signal linked to radiometric accuracy) rather than the studied crop type. Finally, a generally higher F-score value is obtained for the Maize crops (66.7%) than that of the Soybean crops (62.6%).

Table 5. Recall, precision and F-score values aggregated by crop type.

Crop Type	Recall	Precision	F-Score	Undetected Irrigations with NDVI > 0.7
Maize	59.7%	75.3%	66.7%	39.2%
Soybean	54.5%	73.6%	62.6%	59.3%

To examine how the vegetation growth affects the irrigation detection, we chose to examine the correlation between the NDVI, being an indicator for vegetation growth, with the undetected irrigation events. In Table 5, the percentage of the irrigation events not detected due to developed vegetation cover is presented. We calculated it by dividing the number of undetected irrigation events that have a corresponding NDVI value greater than 0.7 by the total number of irrigation events with NDVI > 0.7. The threshold value greater than 0.7 is considered as a good representative of the well-developed vegetation stage, as reported by several sensitivity analysis studies [37,38]. Indeed, Table 5 shows that for Maize crops, 39.2% of the undetected events were justified by the presence of well-developed vegetation cover (NDVI > 0.7). Higher percentage exists over Soybean crops, where 59.3% of the undetected irrigation events were found to be corresponding to well-developed vegetation cover.

To understand the variations in the irrigation detection accuracy as a function of the vegetation development, we investigated, for each crop type, the correlation between the recall metric and the NDVI. Among the three metrics, the recall was chosen to be studied as a function of NDVI, since it reflects the percentage of the irrigation events correctly detected and thus gives an idea about the relation between the failure to detect the irrigation events and the NDVI. To do so, for each crop type, we grouped the irrigation events occurring between June and September on an interval of 20 days. The period from June to September was chosen because this period is usually the period of irrigation for summer crops in our study sites, especially for Maize and Soybean (as shown in Table 1), and corresponds to the beginning of the vegetation development (from moderate to well-developed vegetation cover) in all the sites for both crops. In addition, the grouping of classes on a time interval of 20 days provides a sufficient period to insure the variation in the NDVI values and thus changes in the vegetation stages and characteristics. Therefore, for each crop type (Maize and Soybean), the recall metric was recalculated for each 20-day period as the percentage of detected irrigation events to the total number of irrigations in the same period. The average NDVI values of all the irrigation events was also calculated for each period. Between June and September, we obtained five distinct classes of recall values and their corresponding NDVI values for the five twenty-day interval periods.

Figure 3 shows the variation in the recall metric for the Maize crop, as a function of the NDVI. In Figure 3a, the bar plots represent the recall calculated for each period and the green line shows the variation in the NDVI values. Figure 3a clearly shows that for the Maize crop between June and September, the recall value decreases from about 60% for NDVI values around 0.6 to approximately 40% for NDVI reaching 0.8. Figure 3b shows (for the same samples and periods) the correlation between the recall and the NDVI with a decreasing pattern of recall as NDVI increases and a correlation coefficient (R^2) between the recall and NDVI reaching 0.63. Similarly, for Soybean crops, Figure 4a,b show that the recall value decreases from 100% (all events are detected) for NDVI of 0.4 (low vegetation cover) to reach about 30% for NDVI values beyond 0.7. The correlation coefficient R^2 between the recall and the NDVI for Soybean reaches 0.73 with a decreasing pattern of recall as the NDVI increases.

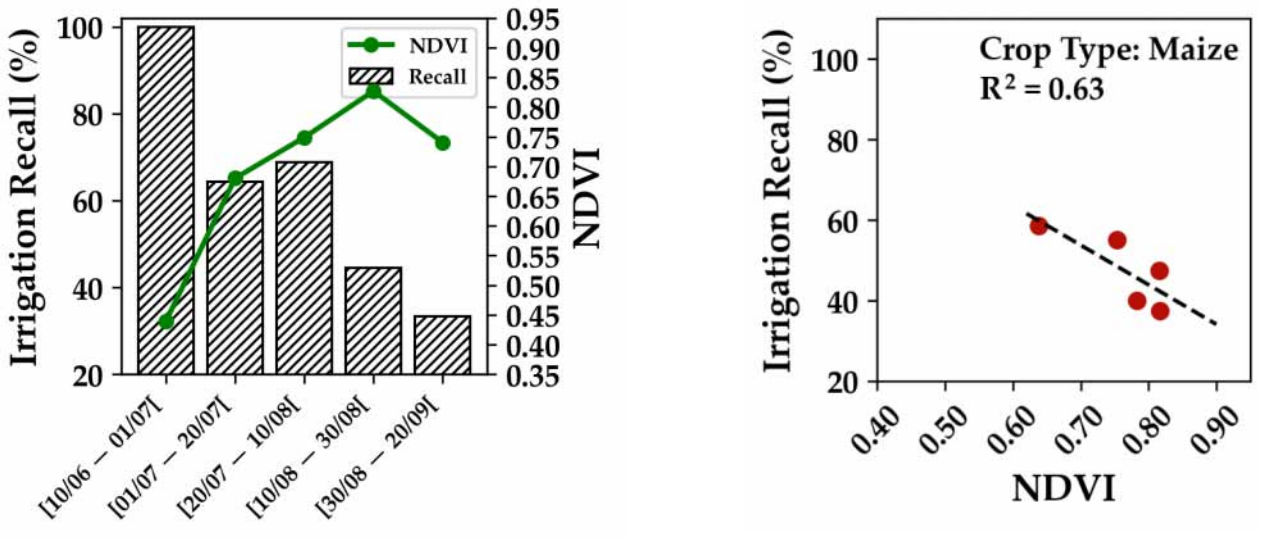

(**a**) (**b**)

Figure 3. (**a**) Dynamics of recall in function of NDVI for Maize crops between September and June. Recall values as bar dashed plots with NDVI in green line; (**b**) recall values plotted against NDVI values. Each point corresponds to the average recall and NDVI, respectively, for the 20-day time interval between June and September.

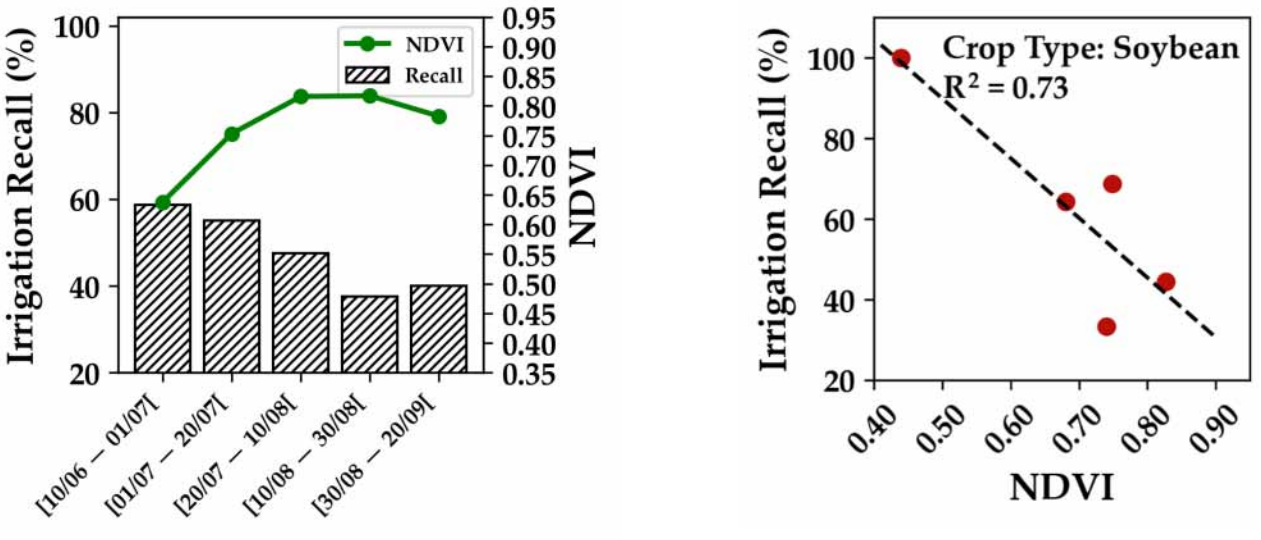

(**a**) (**b**)

Figure 4. (**a**) Dynamics of recall in function of NDVI for Soybean crops between September and June. Recall values as bar dashed plots with NDVI in green line; (**b**) recall values plotted against NDVI values. Each point corresponds to the average recall and NDVI, respectively, for the 20-day time interval between June and September.

For both crop types, it was clearly visible that the development of the vegetation cover constrains the detection of the irrigation events. This could be directly linked to the penetration capabilities of the C-band SAR signal in the well-developed vegetation cover in addition to the effects of the vegetation volume diffusion of the C-band SAR. As shown by several studies, the penetration of the C-band SAR signal to reach the surface soil is highly dependent on the vegetation characteristics, including but not limited to the vegetation height, density and biomass [32,36,38]. Although the vegetation cover constrains the detection of the irrigation events, it remains sometimes possible to detect some of the irrigation events with a highly developed vegetation cover, as the recall value of both crop

types never reaches zero. In fact, for both Maize and Soybean, the vegetation development can constrain the detection of the irrigation events but does not completely prevent it. Indeed, the backscattering SAR signal from well-developed vegetation cover of these two crops remains slightly sensitive to soil moisture but to a lesser degree than that for bare soil or low to moderate vegetation cover [33,40]. The slight variation in the SAR backscattering signal in the case of very well-developed vegetation cover are already considered in the IEDM (the low and moderate irrigation possibilities explained in Section 2.4 with $-0.5 \leq \Delta\sigma^0_{plot} < 1$ dB). Even in the presence of well-developed vegetation cover, the IEDM is still capable of detecting slight variations in the soil moisture to a certain extent and attributes them to irrigation events but with a lower confidence level (low to moderate possibilities). In addition, a possible reason to detect irrigation even when the canopy is well developed is that the S1 satellite has passed at the time of irrigation (this is a possibility, but it is not exclusive). In fact, for crops irrigated by sprinkling, if the satellite passes during the irrigation event it is possible to detect an increase in the radar signal due mainly to water droplets on the leaves.

Unlike the case of Gramineae cereal crops (such as Wheat and Barley) that highly attenuate the C-band SAR signal due to their vertical structure (small leaves, longs stalks and seedheads) and completely prevent the C-band SAR signal from penetrating in developed vegetation, as shown by Bazzi et al. [37], Maize and Soybean crops showed only some limitations in the case of developed vegetation cover where the recall values remained between 30 and 40% for well-developed vegetation. However, the irrigation detection over Soybean crops was more likely to be constrained by the vegetation cover than Maize crops, as the recall value of Soybean had stronger correlation with NDVI (0.73 for Soybean compared to 0.63 for Maize) and a lower value for saturated NDVI (30% for Soybean and 40% for Maize). This slight difference between the Soybean and Maize could be a result of the different developmental characteristics of the Soybean crop as well as the difference in the geometric characteristic of the Soybean plant compared to Maize, which result in more disruption of the C-band SAR signal.

3.4. Effect of the Orbits' Coverages and Number of S1 Images

The last important factor to be discussed in this study is the orbits' coverages and the number of available S1 images used to detect the irrigation events. In fact, it was demonstrated previously by Bazzi et al. [32] that the detection of irrigation events is highly dependent on the revisit time of the S1 satellites. They showed that for bare soil to moderate vegetation cover (NDVI < 0.7), irrigation events could hardly be detected if the time difference between the irrigation event and the next S1 image is more than four days. This time difference decreases to one to two days when the vegetation is developed and the NDVI is greater than 0.7. For this reason, Bazzi et al. [32] recommended using the maximum number of S1 images available from several S1 orbits to guarantee the highest chances of detecting irrigation events. Indeed, overlapping S1 orbits can provide up to 4 S1 images every 6 days with 20 images per month, taking advantage of four possible S1 orbits. However, this condition is not always available for any location on the Earth's surface and is also dependent on the surface area of the studied site to ensure being within the overlapping area of the four S1 orbits.

For this reason, it may happen to have a lower number of S1 images covering a study site, which may reach just a couple of images instead of four in a six-day time interval. Usually, two images in six days are guaranteed from the ascending and descending acquisition modes that cover the same imaged area (using both S1A and S1B). Nevertheless, due to some technical problems or maintenance planning, some S1 images from the same orbit acquisition could be missing, thus leading to less than 10 S1 images per month. For example, in the case of Tarn 2018 and 2019, some images were missing from the source of the ESA website, thus leading to some gaps in the six-day temporal series of the same orbit and a lower number of S1 images per month (seven to eight images per month).

We analyzed the effect of the number of available S1 images per month for each climatic zone separately. Regardless of the crop type, we aggregated the irrigation data based on the number of available images per month and classified them into three classes: the first class corresponds to the plots having less than 10 images per month (7 and 8 images in TR region), the second class corresponds to plots with exactly 10 images per month (dataset in ascending and descending modes) and the third class corresponds to plots with 15 and 20 S1 images per month (full dataset of three to four orbits covering the plots). For the two climatic regions, we calculated the average frequency of irrigation per plot per season. This frequency of irrigation is the ratio between the total number of irrigation events applied to the total number of plots divided by 12 weeks (12 weeks corresponds to 3 months between June and September).

Table 6 summarizes the accuracy metric obtained for different classes of available S1 images for both studied climatic regions. For semi-arid areas, we can observe that the number of S1 images did not greatly affect the detection of the irrigation events. Indeed, while we have no more than 10 images per month for OE, we still obtained a high detection accuracy with high recall values (F-score of 86%). In the case of the Potato plot in LB (with 15 images per month) and for the case of the Maize plots in GR (with 20 images), we obtained nearly similar accuracies to that of the OE, with an F-score reaching 81.2%. These similar accuracies across the semi-arid regions, regardless of the number of images, were expected, since the detection of the change in the soil's water status in dry regions remains possible with irrigations being frequent and rainfall events being rare during the summer. Over all the plots, the frequency of irrigation reached 1 irrigation per week (average of 14 irrigations per plot each season). The high irrigation frequency (up to one irrigation per week) with moderate frequency of S1 images (two images in six days) makes it possible to detect the maximum number of irrigation events even with a lower number of S1 images.

Table 6. Recall, precision and F-score values per class of available S1 images for each climatic region.

Climate	Average Irrigations per Plot per Season	Irrigation Frequency	S1 Images Available per Month	Recall	Precision	F-Score
Semi-Arid	14	One irrigation per week	<10	-	-	-
			10–14	89.5%	82.6%	86.0%
			15–20	76.4%	86.6%	81.2%
Temperate	6	One irrigation per two weeks	<10	46.8%	69.3%	55.9%
			10–14	49.1%	69.0%	57.5%
			15–20	66.7%	76.7%	70.0%

The situation is different in the temperate areas. The results (Table 6) show that the recall (percentage of detected irrigation events) decreases with the decrease in the number of available S1 images and so do the F-score values. For example, plots with less than 10 images per month had an average recall value of 46.8% and an F-score of 55.9%. Plots with 10 images per month had a slightly better average recall value of 49.1% and a slightly higher F-score of 57.4%. Finally, the plots having the maximum number of S1 images per month (20 images) had the highest recall value reaching 66.6% and an F-score of 70%. Thus, in temperate areas, the detection of the irrigation events is highly dependent on the available number of S1 images. This dependency could be explained by the fact that a low number of images accompanied by the low frequency of irrigation in such regions (one irrigation per two weeks) can lead to a higher percentage of the irrigation events being missed if these events do not occur close in time to each available S1 image. In addition, the frequent rainfall with a low number of S1 images can lead to more overlapping between the rainfall and irrigation between the consecutive S1 images, thus limiting the capability of detecting the irrigation event. Therefore, in such temperate climatic conditions, the

likelihood of detecting irrigation events increases when the number of available S1 images is higher.

4. Discussion

In this study, the detection of the irrigation events at the plot scale was assessed using the Sentinel-1 data and a decision tree algorithm (IEDM). Results demonstrated that the IEDM with Sentinel-1 data could provide a good overall performance for irrigation detection. Regardless of some of the presented limitations of the IEDM performance across climatic regions and studied crops, the IEDM combined with Sentinel-1 could still be efficient to detect irrigation events. However, other limitation factors could also be discussed to assess better the performance of the IEDM with S1.

The IEDM was applied to all agricultural plots regardless of the soil type of each plot. The effect of the irrigation on the soil wetness degree could be also correlated to the soil type of the agricultural plot. Indeed, soil texture and its field capacity, which is the amount of water content held in the soil after excess water caused by rainfall or irrigation, can have a significant impact on the detection of the irrigation events. This is mainly related to the soil depletion, dry out and evaporation rates that vary between soil types and climatic conditions. Usually, soils that have more capacity to retain water in their top layers are more likely to have better detection of the irrigation events, especially in arid and semi-arid areas where the dry out of the soil is rapid due to high evaporation intensity. In this case, even if the surface soil water is very low, the overall soil water in the lower soil depth is not necessarily low. The condition of the rapid dry out of the surface soil (depending on soil texture and climate) and the different soil water content between top layers and deep layers generate the discussion of two principal points for irrigation detection using S1 and the IEDM: (1) the temporal resolution of the used sensor and (2) the penetration of the used SAR signal.

First, the rapid dry out of the soil means that the used sensor should have higher temporal resolution that may be useful to detect rapid change in the soil moisture content (increase due to irrigation and decrease after due to dry out). As discussed in the manuscript and validated in previous studies [32,34,35], the maximum time delay between the irrigation event and the next S1 image to detect the irrigation event must not exceed 4 days. The effect of the satellite temporal resolution on the irrigation detection was assessed by several studies [36,37]. Le Page et al. [34], Ouaadi et al. [35] and Bazzi et al. [37] showed that beyond three to four days after the irrigation, it becomes difficult to detect the effect of an irrigation event on the S1 backscattering signal, and thus the irrigation could hardly be detected. This fact was also proved by El Hajj et al. [36] using the X-band SAR data, where they showed that it was difficult to detect an irrigation event occurring three to four days before the SAR acquisition. This leads to the fact that for efficient detection of all irrigation events, the temporal resolution of the SAR sensor must be at most less than 4 days. Finally, the revisit time of the SAR constellation is one the most important challenges to detect the irrigation events.

The second main point regarding the dry out of the surface soil and the difference between surface and deep-water content is the penetration of the used SAR band to detect the wetness degree of the soil. In the case of S1 with a C-band signal at a wavelength of about 5 cm, only the wetness degree of the first 5 cm of the soil could be measured. In fact, even with such limited penetration, the S1 sensor, as shown in this paper, could still detect irrigation events with good accuracy. Nevertheless, it is well known that using SAR signals with higher wavelengths could be more adequate to measure soil water content for soil layers deeper than 5 cm. For example, the L-band SAR signal having a wavelength reaching about 24 cm has higher penetration capabilities than the C-band and can reflect better the soil water status and its variation after the irrigation events. A recent study comparing between the C- and L-bands for irrigation detection demonstrated that the L-band performs better than the C-band in irrigation detection and shows higher variability to the variation in the soil water content than the C-band [37]. In Bazzi et al. [37], they showed that between

wet and dry soil, the L-band can vary from −11 dB for wet soil due to irrigation to less than −18 dB when the soil is completely dry (difference of about 7 dB). For the C-band, the variation was less than that of the L-band, where the backscattering SAR signal could vary from −10 dB to −14 dB (difference of 4 dB) between wet and dry soil. Their study also demonstrated that the correlation between the SAR backscattering signal and the wetness degree of the soil was higher for the L-band than C-band. They concluded then that even though the C-band could still be used to detect irrigation events and wetness degrees, the L-band shows superior capabilities compared to the C-band. Unfortunately, until now the L-band remains for non-commercial use and operational L-band SAR sensors in free and open access modes are not available, which makes the use of the L-band sensor for irrigation detection in operational modes inadequate. However, future planned L-band sensors can open the way toward better detection of irrigation events by integrating the L-band SAR data in the IEDM instead of the C-band SAR data. This integration may also necessitate the re-calibration of the IEDM threshold values of the decision tree to be more adequate with the L-band SAR signal.

Another point to discuss regarding the IEDM and the S1 is the irrigation system used at the plot scale. In this study, almost all the plots were irrigated by the common sprinkler irrigation technique. Previously, Bazzi et al. [32] reported a similar capability of the S1 data to detect irrigation using the gravity irrigation technique. Drip irrigation, which is becoming more common now to reduce the water consumption and increase the water use efficiency, is not yet analyzed. In this study, only a few irrigation events in the Greece Maize crops were performed using drip irrigation. No specific observation was remarked for these irrigation events that were also detected in the study. However, the absence of a robust database of drip irrigation prevents us from drawing out robust conclusions regarding the capability to detect these irrigation events using the S1 and the IEDM. A study performed by Soulis et al. [41] assessed the effect of the positioning of the soil moisture sensors placed in soil on the soil moisture values in the drip irrigation context. They showed that the irrigation efficiency was significantly affected by the placement of the soil water content sensor (depth of sensor). Specifically, the sensor placement on the irrigation efficiency had an efficiency as high as 16%. Back to the SAR data, this means that the penetration of the SAR signal (at 5 or 24 cm) can play an important role in the detection of the irrigation events in drip irrigation cases, as the drip irrigation is more targeted to the plants.

The last point to discuss in this paper is the operational use of the IEDM to serve as a generic tool for irrigation detection. In fact, the IEDM was first proposed as a near-real-time model to detect irrigation events and thus can serve as an irrigation detection tool during the growing season. The data used to detect irrigation events in the S1 image of date (t) do not rely on the future captured S1 image of date t + i but on the previous S1 images captured before the time t (mainly on t-1). The efficiency and rapidity of the IEDM to detect an irrigation event is thus dependent on the delivery time of S1 images, which are usually delivered in a "fast 24 h" delivery mode. Therefore, the implementation of the IEDM in an operational pipeline tool can guarantee the detection of the irrigation event in real time after the availability of the S1 image. Moreover, the IEDM requires the agricultural plots' boundaries to calculate the SAR backscattering signals at plot scales. These data, which are sometimes available for some countries, could also be generated using a simple image segmentation technique of an NDVI time series to obtain an accepted map of the agricultural plots' boundaries if they are not available at the national scale. Current tools such as the LPIS (land-parcel identification system) could help obtain the agricultural plots' boundaries used to calculate the SAR signal at both plot and grid scales (10 km × 10 km) required by the IEDM.

5. Conclusions

This study presented a detailed assessment of detecting irrigation events at the plot scale using the S1 time series data and a change detection algorithm (IEDM). The IEDM

was applied using S1 time series over five semi-arid and temperate study sites in Europe and the Middle East and across several major summer crops.

The main findings showed that the accuracy of the irrigation detection reaches 85% for semi-arid areas, higher than that for temperate areas reaching 53%. Developed vegetation cover was found to be an important constraint in the detection of irrigation events, where the irrigation detection accuracy decreased from about 60% for moderate vegetation cover (NDVI < 0.60) to less than 40% when the NDVI reached values beyond 0.7. The main results also demonstrated the dependency of the irrigation detection accuracy on the availability of the S1 images (number of used S1 images in the S1 time series), especially over temperate areas. The effect of the availability of S1 images was of great importance to analyze, especially with the loss of the S1B satellite from the S1 constellation which will reduce the S1 revisit time. Future assessment of the IEDM may include the analysis of irrigation detection accuracy with respect to soil types and irrigation techniques.

Despite some limitations regarding the climatic context and the vegetation development, the IEDM proved to be a powerful tool for irrigation detection at the plot scale. The IEDM, which could be implemented in a near-real-time operational application, may automatize the detection of irrigation events at the plot scale and help authorities better understand the water consumption rates in irrigated agriculture, especially for regions encountering illegal water abstractions and water scarcity.

Author Contributions: Conceptualization, H.B. and N.B.; Data curation, H.B., S.N., H.J., M.L.P., I.F. and M.S.; Formal analysis, H.B., N.B., S.N. and H.J.; Methodology, H.B., N.B., S.N. and M.Z.; Software, H.B.; Supervision, N.B. and H.J.; Validation, H.B., N.B., M.L.P., I.F. and M.S.; Writing—original draft, H.B., N.B. and S.N.; Writing—review and editing, N.B., H.J., M.L.P., M.Z., I.F. and M.S. All authors have read and agreed to the published version of the manuscript.

Funding: This research received funding from the French Space Study Center (CNES, TOSCA 2022 project), the French Agency for Ecological Transition (ADEME, RSEAU project) and the National Research Institute for Agriculture, Food and the Environment (INRAE). H.J. acknowledges funds from Google.org and the Tides Foundation, award 103808. This research was also funded by the project HubIS under the PRIMA 2019 program of the European Commission (HORIZON EUROPE).

Data Availability Statement: Sentinel-1 data are available via the Copernicus open-access hub (https://scihub.copernicus.eu/dhus/#/home (accessed on 15 September 2022)). Sentinel-2 data are available on the Theia French Land Data Center website (https://www.theia-land.fr/en/product/sentinel-2-surface-reflectance/, accessed on 15 September 2022).

Acknowledgments: The authors wish to thank the French Space Study Center (CNES, TOSCA 2022), the French Agency for Ecological Transition (ADEME, RSEAU project), and the National Research Institute for Agriculture, Food and the Environment (INRAE) for supporting this work. The authors would like to thank Giorgios Tziatzios and Nicolas Dalezios from the University of Thessaly, Greece, for providing valuable terrain data. The authors would like to also thank the European Space Agency (ESA) for providing the S1 images and the French Land Data Center (Theia) for providing the S2 images.

Conflicts of Interest: The authors declare no conflict of interest.

References

1. Kummu, M.; Guillaume, J.H.; de Moel, H.; Eisner, S.; Flörke, M.; Porkka, M.; Siebert, S.; Veldkamp, T.I.; Ward, P.J. The World's Road to Water Scarcity: Shortage and Stress in the 20th Century and Pathways towards Sustainability. *Sci. Rep.* **2016**, *6*, 38495. [CrossRef] [PubMed]
2. Tilman, D.; Clark, M. Food, Agriculture & the Environment: Can We Feed the World & Save the Earth? *Daedalus* **2015**, *144*, 8–23.
3. Richardson, K.J.; Lewis, K.H.; Krishnamurthy, P.K.; Kent, C.; Wiltshire, A.J.; Hanlon, H.M. Food Security Outcomes under a Changing Climate: Impacts of Mitigation and Adaptation on Vulnerability to Food Insecurity. *Clim. Chang.* **2018**, *147*, 327–341. [CrossRef]
4. Schultz, G.A.; Engman, E.T. *Remote Sensing in Hydrology and Water Management*; Springer Science & Business Media: Berlin/Heidelberg, Germany, 2012; ISBN 3-642-59583-9.
5. Bastiaanssen, W.G.; Molden, D.J.; Makin, I.W. Remote Sensing for Irrigated Agriculture: Examples from Research and Possible Applications. *Agric. Water Manag.* **2000**, *46*, 137–155. [CrossRef]

6. Ozdogan, M.; Gutman, G. A New Methodology to Map Irrigated Areas Using Multi-Temporal MODIS and Ancillary Data: An Application Example in the Continental US. *Remote Sens. Environ.* **2008**, *112*, 3520–3537. [CrossRef]
7. Bazzi, H.; Baghdadi, N.; Ienco, D.; El Hajj, M.; Zribi, M.; Belhouchette, H.; Escorihuela, M.J.; Demarez, V. Mapping Irrigated Areas Using Sentinel-1 Time Series in Catalonia, Spain. *Remote Sens.* **2019**, *11*, 1836. [CrossRef]
8. Bazzi, H.; Baghdadi, N.; Amin, G.; Fayad, I.; Zribi, M.; Demarez, V.; Belhouchette, H. An Operational Framework for Mapping Irrigated Areas at Plot Scale Using Sentinel-1 and Sentinel-2 Data. *Remote Sens.* **2021**, *13*, 2584. [CrossRef]
9. Dari, J.; Brocca, L.; Quintana-Seguí, P.; Escorihuela, M.J.; Stefan, V.; Morbidelli, R. Exploiting High-Resolution Remote Sensing Soil Moisture to Estimate Irrigation Water Amounts over a Mediterranean Region. *Remote Sens.* **2020**, *12*, 2593. [CrossRef]
10. Xie, Y.; Lark, T.J. Mapping Annual Irrigation from Landsat Imagery and Environmental Variables across the Conterminous United States. *Remote Sens. Environ.* **2021**, *260*, 112445. [CrossRef]
11. Motte, E.; Zribi, M.; Fanise, P.; Egido, A.; Darrozes, J.; Al-Yaari, A.; Baghdadi, N.; Baup, F.; Dayau, S.; Fieuzal, R. GLORI: A GNSS-R Dual Polarization Airborne Instrument for Land Surface Monitoring. *Sensors* **2016**, *16*, 732. [CrossRef]
12. Ienco, D.; Interdonato, R.; Gaetano, R.; Minh, D.H.T. Combining Sentinel-1 and Sentinel-2 Satellite Image Time Series for Land Cover Mapping via a Multi-Source Deep Learning Architecture. *ISPRS J. Photogramm. Remote Sens.* **2019**, *158*, 11–22. [CrossRef]
13. Baghdadi, N.; El Hajj, M.; Choker, M.; Zribi, M.; Bazzi, H.; Vaudour, E.; Gilliot, J.-M.; Ebengo, D.M. Potential of Sentinel-1 Images for Estimating the Soil Roughness over Bare Agricultural Soils. *Water* **2018**, *10*, 131. [CrossRef]
14. Bazzi, H.; Baghdadi, N.; El Hajj, M.; Zribi, M. Potential of Sentinel-1 Surface Soil Moisture Product for Detecting Heavy Rainfall in the South of France. *Sensors* **2019**, *19*, 802. [CrossRef] [PubMed]
15. Bousbih, S.; Zribi, M.; Pelletier, C.; Gorrab, A.; Lili-Chabaane, Z.; Baghdadi, N.; Ben Aissa, N.; Mougenot, B. Soil Texture Estimation Using Radar and Optical Data from Sentinel-1 and Sentinel-2. *Remote Sens.* **2019**, *11*, 1520. [CrossRef]
16. Gao, Q.; Zribi, M.; Escorihuela, M.J.; Baghdadi, N.; Segui, P.Q. Irrigation Mapping Using Sentinel-1 Time Series at Field Scale. *Remote Sens.* **2018**, *10*, 1495. [CrossRef]
17. Bazzi, H.; Baghdadi, N.; Zribi, M. Comparative Analysis between Two Operational Irrigation Mapping Models over Study Sites in Mediterranean and Semi-Oceanic Regions. *Water* **2022**, *14*, 1341. [CrossRef]
18. de Albuquerque, A.O.; de Carvalho, O.L.F.; e Silva, C.R.; de Bem, P.P.; Trancoso Gomes, R.A.; Borges, D.L.; Guimarães, R.F.; Pimentel, C.M.M.; de Carvalho Júnior, O.A. Instance Segmentation of Center Pivot Irrigation Systems Using Multi-Temporal SENTINEL-1 SAR Images. *Remote Sens. Appl. Soc. Environ.* **2021**, *23*, 100537. [CrossRef]
19. Elwan, E.; Le Page, M.; Jarlan, L.; Baghdadi, N.; Brocca, L.; Modanesi, S.; Dari, J.; Quintana Seguí, P.; Zribi, M. Irrigation Mapping on Two Contrasted Climatic Contexts Using Sentinel-1 and Sentinel-2 Data. *Water* **2022**, *14*, 804. [CrossRef]
20. Abubakar, M.; Chanzy, A.; Pouget, G.; Flamain, F.; Courault, D. Detection of Irrigated Permanent Grasslands with Sentinel-2 Based on Temporal Patterns of the Leaf Area Index (LAI). *Remote Sens.* **2022**, *14*, 3056. [CrossRef]
21. Massari, C.; Modanesi, S.; Dari, J.; Gruber, A.; De Lannoy, G.J.M.; Girotto, M.; Quintana-Seguí, P.; Le Page, M.; Jarlan, L.; Zribi, M.; et al. A Review of Irrigation Information Retrievals from Space and Their Utility for Users. *Remote Sens.* **2021**, *13*, 4112. [CrossRef]
22. Dari, J.; Quintana-Seguí, P.; Morbidelli, R.; Saltalippi, C.; Flammini, A.; Giugliarelli, E.; Escorihuela, M.J.; Stefan, V.; Brocca, L. Irrigation Estimates from Space: Implementation of Different Approaches to Model the Evapotranspiration Contribution within a Soil-Moisture-Based Inversion Algorithm. *Agric. Water Manag.* **2022**, *265*, 107537. [CrossRef]
23. Dari, J.; Quintana-Seguí, P.; Escorihuela, M.J.; Stefan, V.; Brocca, L.; Morbidelli, R. Detecting and Mapping Irrigated Areas in a Mediterranean Environment by Using Remote Sensing Soil Moisture and a Land Surface Model. *J. Hydrol.* **2021**, *596*, 126129. [CrossRef]
24. Baghdadi, N.; King, C.; Chanzy, A.; Wigneron, J.P. An Empirical Calibration of the Integral Equation Model Based on SAR Data, Soil Moisture and Surface Roughness Measurement over Bare Soils. *Null* **2002**, *23*, 4325–4340. [CrossRef]
25. Kornelsen, K.C.; Coulibaly, P. Advances in Soil Moisture Retrieval from Synthetic Aperture Radar and Hydrological Applications. *J. Hydrol.* **2013**, *476*, 460–489. [CrossRef]
26. El Hajj, M.; Baghdadi, N.; Zribi, M.; Bazzi, H. Synergic Use of Sentinel-1 and Sentinel-2 Images for Operational Soil Moisture Mapping at High Spatial Resolution over Agricultural Areas. *Remote Sens.* **2017**, *9*, 1292. [CrossRef]
27. Baghdadi, N.; Abou Chaaya, J.; Zribi, M. Semiempirical Calibration of the Integral Equation Model for SAR Data in C-Band and Cross Polarization Using Radar Images and Field Measurements. *IEEE Geosci. Remote Sens. Lett.* **2011**, *8*, 14–18. [CrossRef]
28. El Hajj, M.; Baghdadi, N.; Zribi, M.; Belaud, G.; Cheviron, B.; Courault, D.; Charron, F. Soil Moisture Retrieval over Irrigated Grassland Using X-Band SAR Data. *Remote Sens. Environ.* **2016**, *176*, 202–218. [CrossRef]
29. He, B.; Xing, M.; Bai, X. A Synergistic Methodology for Soil Moisture Estimation in an Alpine Prairie Using Radar and Optical Satellite Data. *Remote Sens.* **2014**, *6*, 10966–10985. [CrossRef]
30. Salmon, J.M.; Friedl, M.A.; Frolking, S.; Wisser, D.; Douglas, E.M. Global Rain-Fed, Irrigated, and Paddy Croplands: A New High Resolution Map Derived from Remote Sensing, Crop Inventories and Climate Data. *Int. J. Appl. Earth Obs. Geoinf.* **2015**, *38*, 321–334. [CrossRef]
31. Pageot, Y.; Baup, F.; Inglada, J.; Baghdadi, N.; Demarez, V. Detection of Irrigated and Rainfed Crops in Temperate Areas Using Sentinel-1 and Sentinel-2 Time Series. *Remote Sens.* **2020**, *12*, 3004. [CrossRef]
32. Bazzi, H.; Baghdadi, N.; Fayad, I.; Charron, F.; Zribi, M.; Belhouchette, H. Irrigation Events Detection over Intensively Irrigated Grassland Plots Using Sentinel-1 Data. *Remote Sens.* **2020**, *12*, 4058. [CrossRef]

33. Bazzi, H.; Baghdadi, N.; Fayad, I.; Zribi, M.; Belhouchette, H.; Demarez, V. Near Real-Time Irrigation Detection at Plot Scale Using Sentinel-1 Data. *Remote Sens.* **2020**, *12*, 1456. [CrossRef]
34. Le Page, M.; Jarlan, L.; El Hajj, M.M.; Zribi, M.; Baghdadi, N.; Boone, A. Potential for the Detection of Irrigation Events on Maize Plots Using Sentinel-1 Soil Moisture Products. *Remote Sens.* **2020**, *12*, 1621. [CrossRef]
35. Ouaadi, N.; Jarlan, L.; Khabba, S.; Ezzahar, J.; Le Page, M.; Merlin, O. Irrigation Amounts and Timing Retrieval through Data Assimilation of Surface Soil Moisture into the FAO-56 Approach in the South Mediterranean Region. *Remote Sens.* **2021**, *13*, 2667. [CrossRef]
36. Hajj, M.E.; Baghdadi, N.; Belaud, G.; Zribi, M.; Cheviron, B.; Courault, D.; Hagolle, O.; Charron, F. Irrigated Grassland Monitoring Using a Time Series of TerraSAR-X and COSMO-SkyMed X-Band SAR Data. *Remote Sens.* **2014**, *6*, 10002–10032. [CrossRef]
37. Bazzi, H.; Baghdadi, N.; Charron, F.; Zribi, M. Comparative Analysis of the Sensitivity of SAR Data in C and L Bands for the Detection of Irrigation Events. *Remote Sens.* **2022**, *14*, 2312. [CrossRef]
38. Baghdadi, N.N.; El Hajj, M.; Zribi, M.; Fayad, I. Coupling SAR C-Band and Optical Data for Soil Moisture and Leaf Area Index Retrieval over Irrigated Grasslands. *IEEE J. Sel. Top. Appl. Earth Obs. Remote Sens.* **2015**, *9*, 1229–1243. [CrossRef]
39. Inglada, J.; Vincent, A.; Arias, M.; Tardy, B.; Morin, D.; Rodes, I. Operational High Resolution Land Cover Map Production at the Country Scale Using Satellite Image Time Series. *Remote Sens.* **2017**, *9*, 95. [CrossRef]
40. Joseph, A.T.; van der Velde, R.; O'Neill, P.E.; Lang, R.; Gish, T. Effects of Corn on C- and L-Band Radar Backscatter: A Correction Method for Soil Moisture Retrieval. *Remote Sens. Environ.* **2010**, *114*, 2417–2430. [CrossRef]
41. Soulis, K.X.; Elmaloglou, S.; Dercas, N. Investigating the Effects of Soil Moisture Sensors Positioning and Accuracy on Soil Moisture Based Drip Irrigation Scheduling Systems. *Agric. Water Manag.* **2015**, *148*, 258–268. [CrossRef]